Supporting Information

Hollow-porous fibers for intrinsically thermal insulating textiles and wearable electronics with ultrahigh workable sensitivity

Yunfei Yu,[a] Guangchao Zheng,[b] Kun Dai,* Wei Zhai,[a] Kangkang Zhou,[a] Yanyan Jia,[a] Guoqiang Zheng,[a] Zhicheng Zhang,*[c] Chuntai Liu,[a] and Changyu Shen[a]

[a]School of Materials Science and Engineering, Key Laboratory of Materials Processing and Mold (Zhengzhou University), Ministry of Education; Henan Key Laboratory of Advanced Nylon Materials and Application (Zhengzhou University), Zhengzhou University, Zhengzhou, 450001, P. R. China
E-mail: kundai@zzu.edu.cn (K. Dai)

[b]School of Physics and Microelectronics, Zhengzhou University, Zhengzhou, 450001, P. R. China

[c]Tianjin Key Laboratory of Molecular Optoelectronic Sciences, Department of Chemistry, School of Science, Tianjin University & Collaborative Innovation Center of Chemical Science and Engineering, Tianjin 300072, P. R. China
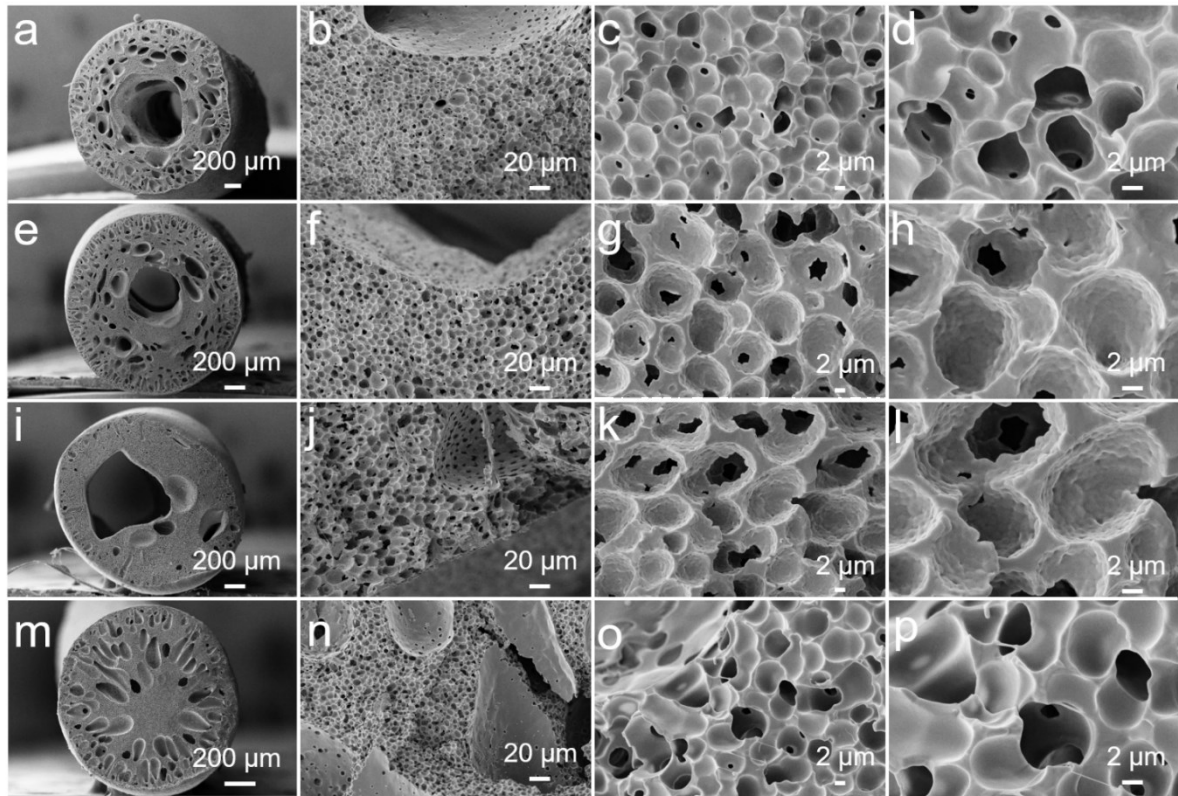E-mail: zczhang19@tju.edu.cn (Z. Zhang)

Fig. S1. Cross section SEM images of TPU fibers. a-d) TPU-2.1; e-h) TPU-1.9; i-l) TPU-1.6; m-p) TPU-1.2.

Fig. S1a-d and Fig. S1e-h illustrate the cross-sections of TPU-D2.1 and TPU-D1.9, respectively. TPU-D1.9 has a similar cross-sectional structure as TPU-D2.1, and the diameter of the hollow structure is about 650 μm, the density and porosity of the sample are 0.35 g/cm^3 and 68.2%, respectively. As for the TPU-D1.6, its hollow structure is not a standard circle shape (Fig. S1i-l). No obvious hollow structure is observed in TPU-D1.2 (Fig. S1m-p), nevertheless, a porous structure is still obtained. All the densities and porosities of the samples are summarized and listed in Table S1.
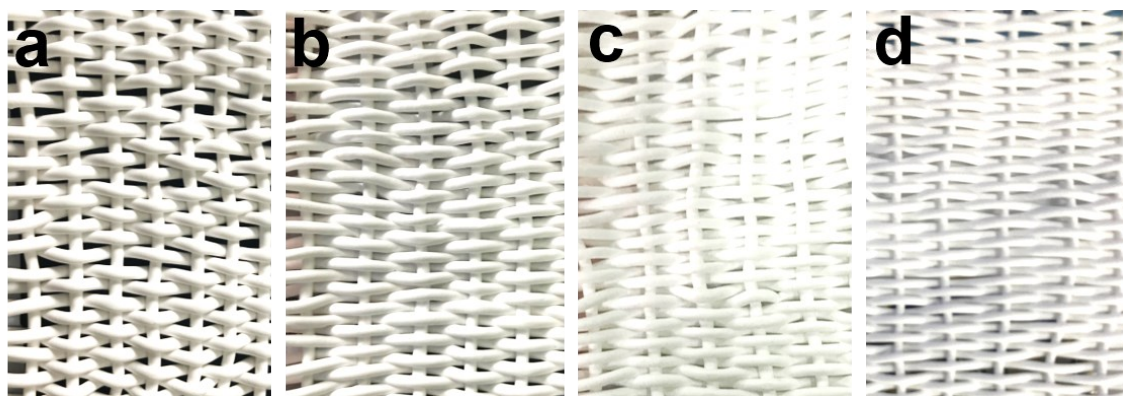
Fig. S2. Photographs of textiles woven by porous TPU fibers with different diameters, a) 2.1, b) 1.9, c) 1.6 and d) 1.2 mm, respectively.
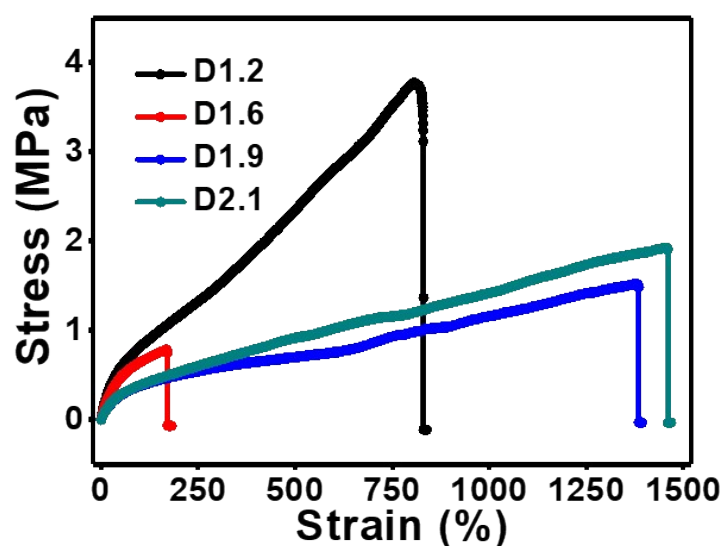

Fig. S3. Typical stress-strain curves of different TPU fibers.

For TPU-D2.1, D1.9, D1.6 and D1.2, their elongations at break and strengths are 1468%, 1387%, 175%, 807% and 1.92, 1.52, 0.81, 3.76 MPa, respectively. Overall, the elongation at break of the fiber decreases with the increase of the diameter, except the TPU-D1.6. It is possible that the irregular hollow structure formed in TPU-D1.6 makes the wall of one side of the tube-like fiber become rather thinner (Fig. S1i), resulting in the reduction in elongation at break (175%), while it still meets the requirements of wearable devices.
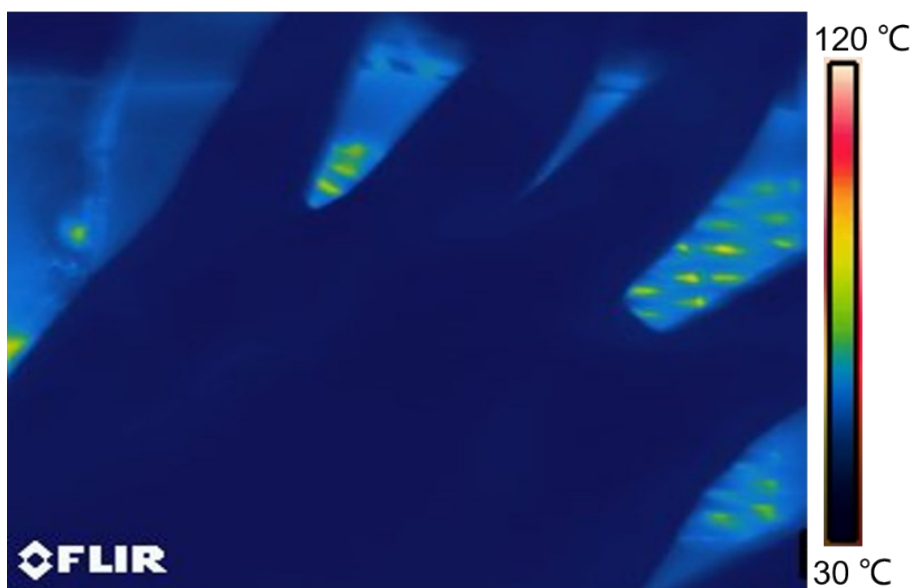
Fig. S4. Thermal infrared image of a hand of a volunteer on the heated textiles.
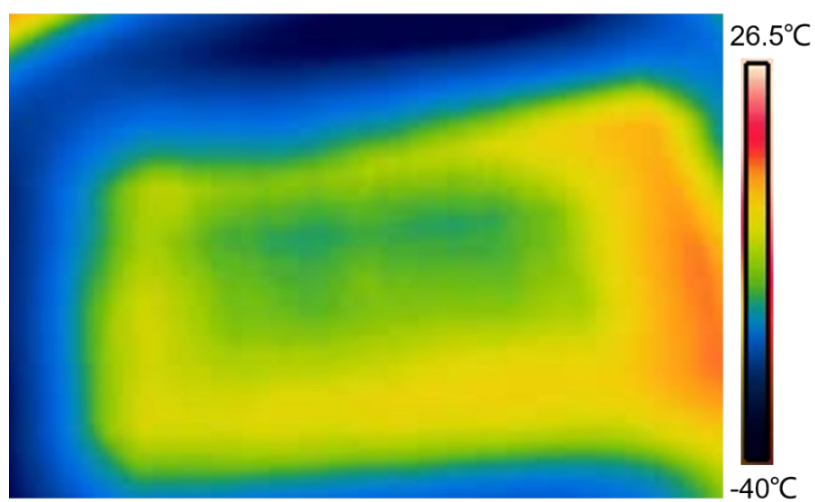

Fig. S5. Thermal infrared image of TPU-D2.1-1 placed on an iron plate at -40 ºC.

The temperature of the iron plate is cooled by liquid nitrogen to below -40 ºC. Then TPU-D2.1-1 is placed on the iron plate. After 3 min, the temperature of the textile remained stable in the photos recorded by the infrared camera.
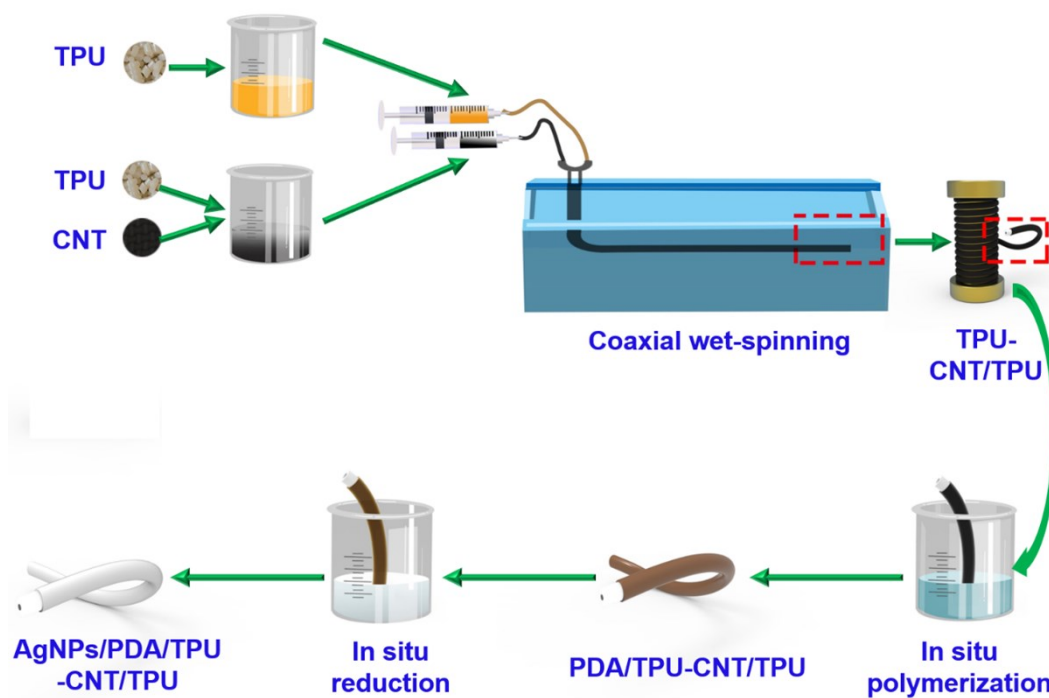
Fig. S6. Schematic diagram of the preparation processes of conductive hollow-porous AgNPs/PDA/CNT-TPU/TPU fiber.
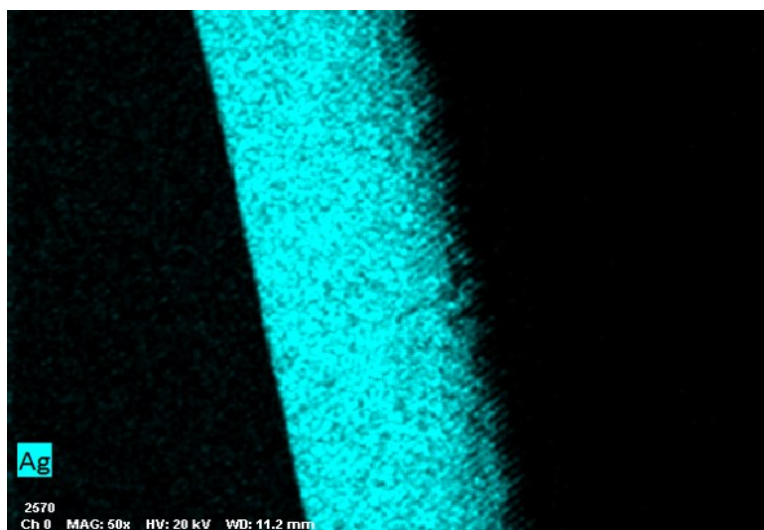

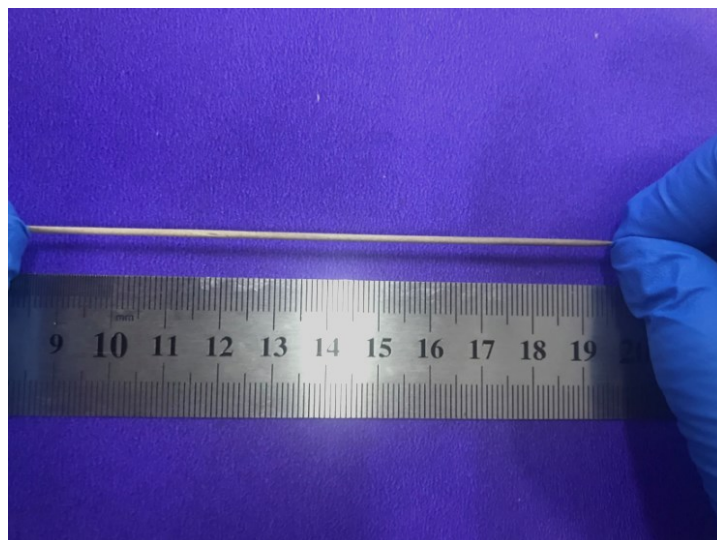**Fig. S7.** Ag element distribution on the cross section of the fiber.

Fig. S8. Photograph of the APTTF sample in stretching.
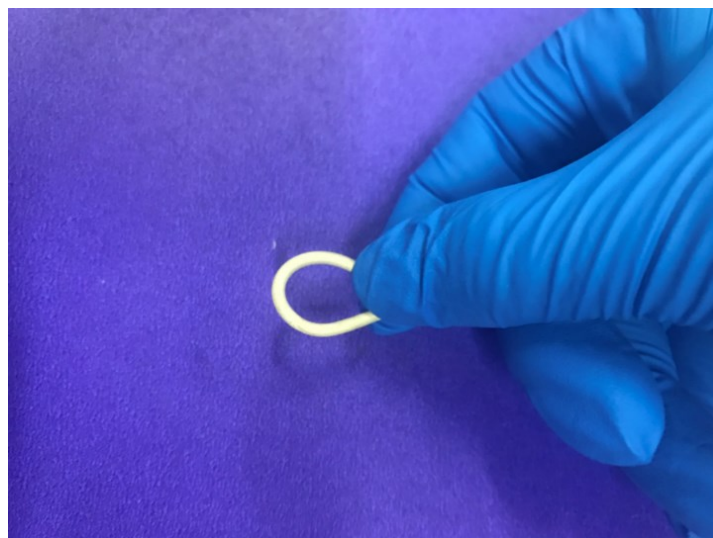

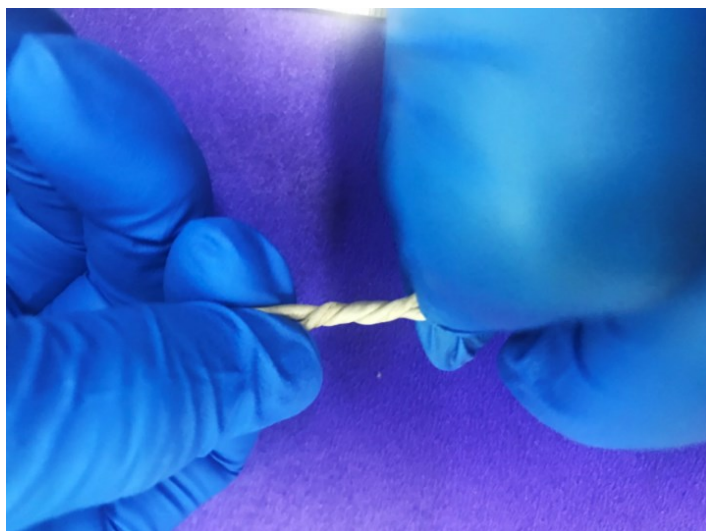**Fig. S9.** Photograph of the APTTF in bending.

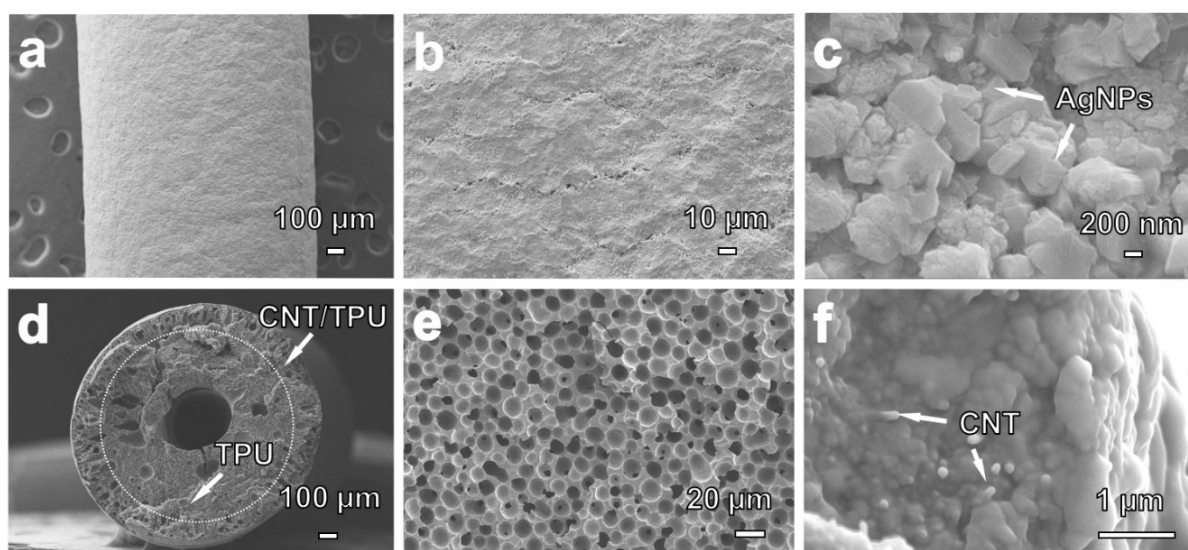**Fig. S10.** Photograph of the APTTF sample in twisting.

Fig. S11. SEM images of APTTF, a-c) surface section; d-f) cross section, including the CNT/TPU layer, TPU layer and the hollow core.

We can clearly observe (Fig. S11d-f) that APTTF has a distinct hollow-porous structure with an empty perforation diameter of about 496 µm and an overall fiber diameter of about 1.76 mm.
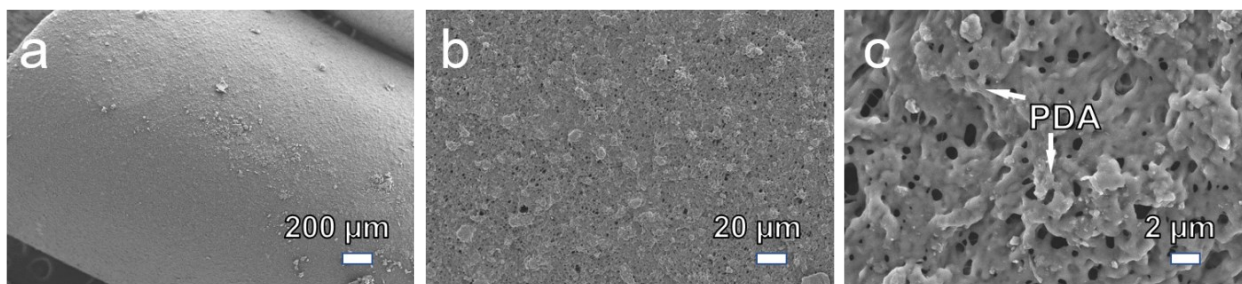
Fig. S12. SEM of PDA/CNT-TPU/TPU fibers at different magnifications: a) 100 times; b) 1000 times; c) 5000 times.
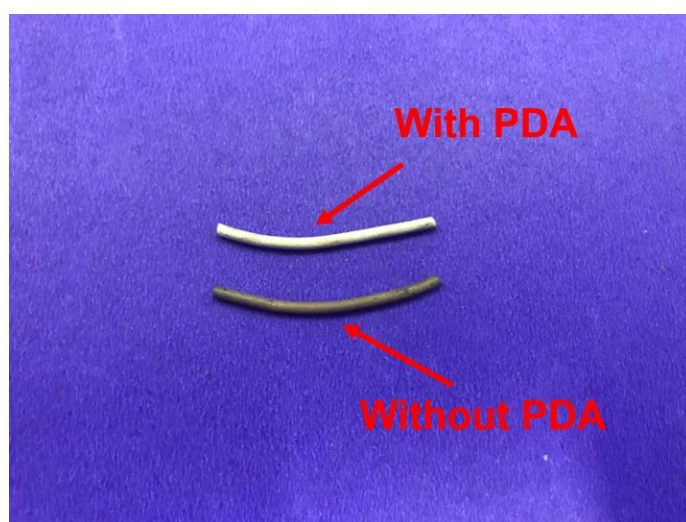

Fig. S13. Photograph of the fiber with or without PDA.

Color changes of the fibers with or without PDA are compared in Fig. S13. The results indicate that the fiber without PDA is oxidized and turns to be black, while the APTTF with PDA appears white. Furthermore, resistance test demonstrates that the resistance of the PDA-free fiber is 5 MΩ, while the resistance of the APTTF is only 5 Ω and keeps stable in air over 6 months. This phenomenon is attributed to the reductive nature of PDA and its contribution to the fixation of inorganic particles, which is beneficial to the adhesion of AgNPs on the surface of the fiber.
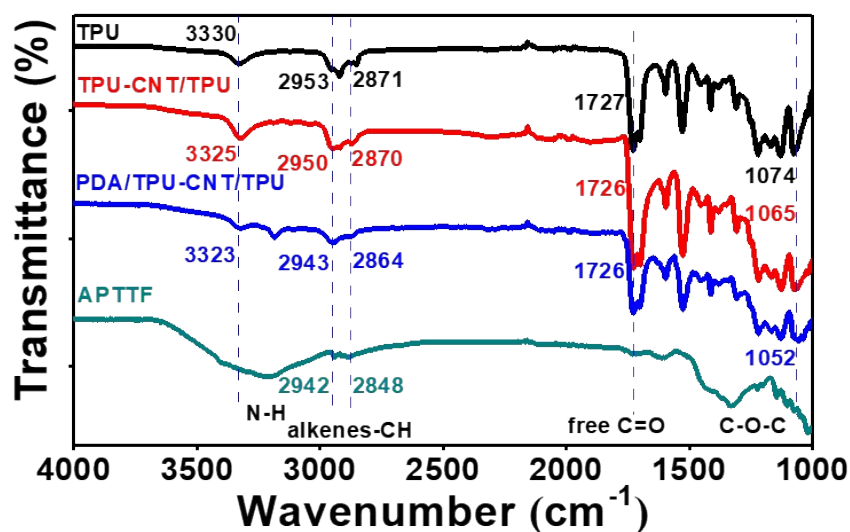
Fig. S14. FTIR of the TPU fiber, TPU-CNT/TPU fiber, PDA/TPU-CNT/TPU fiber and APTTF.

In Fig. S14, five characteristic peaks of TPU at 1074, 1727, 2871, 2953 and 3330 cm^{-1} belong to C-O-C stretching vibration peak, -C=O free characteristic peak, -CH stretching vibration peak (2871 cm^{-1}, 2953 cm^{-1}) and telescopic vibration of -NH, respectively. For the TPU-CNT/TPU composite, the above characteristic peaks are transferred to 1065, 1726, 2870, 2950 and 3325 cm^{-1}, respectively. After the polymerization of PDA, the peaks are transferred to 1052, 1726, 2864, 2943 and 3323 cm^{-1}, respectively. Finally, after the in-situ synthesis of AgNPs, the C-O-C stretching vibration peak, -C=O free characteristic peak and the stretching vibration of -NH disappears, while the stretching vibration peak of -CH shifts to 2848 and 2942 cm^{-1}. These changes of the above characteristic peak indicate that a strong interaction indeed exists between TPU, CNT, PDA and AgNPs of the APTTF.
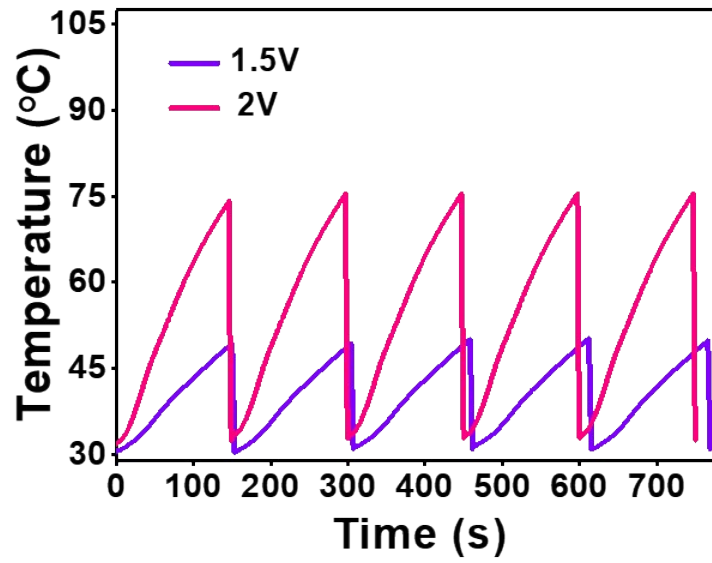
Fig. S15. Five-cycle temperature change of APTTF under the voltage of 1.5 V and 2 V for 150 s.
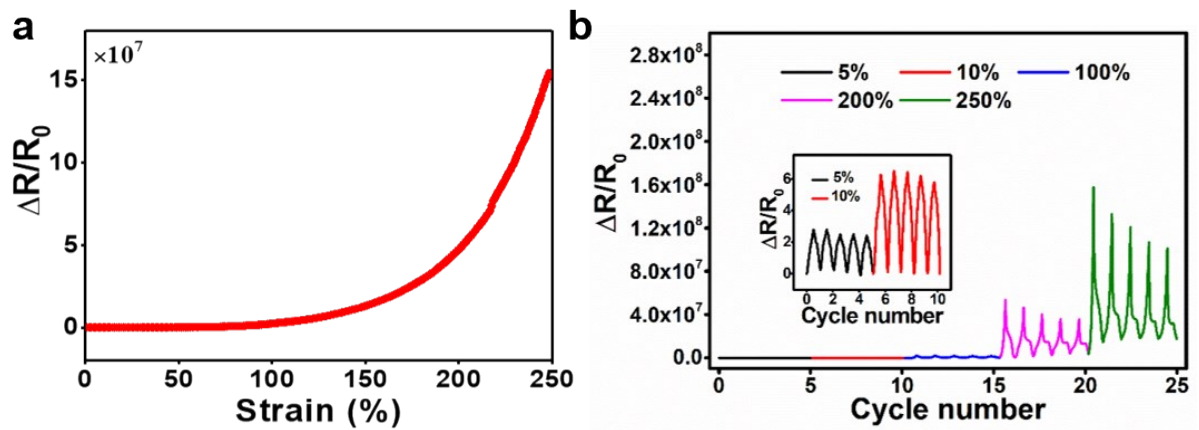

Fig. S16. (a) Changes in $\Delta R/R_0$ versus strain of APTTF strain sensor. (b) Electromechanical properties of our coaxial fiber under cyclic stretching-releasing deformation at various applied strains.
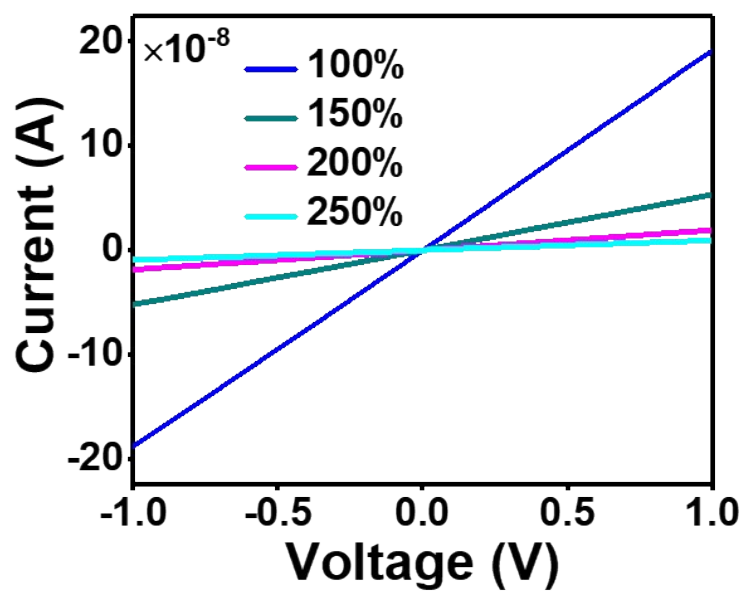
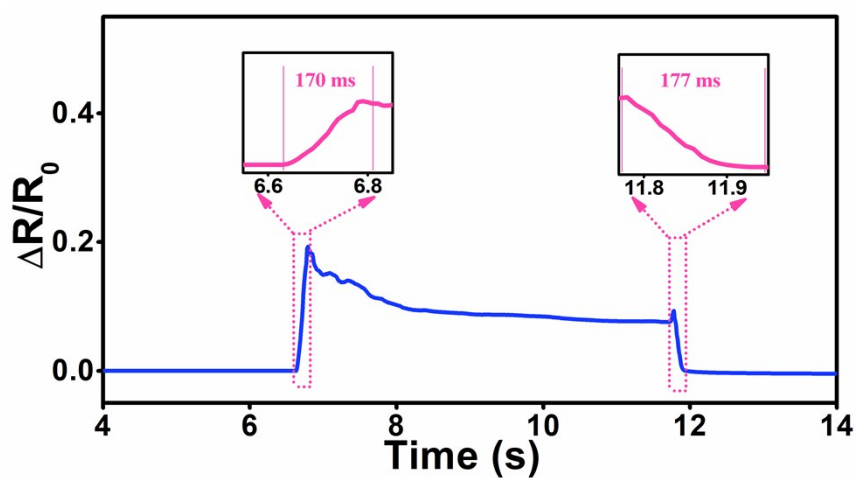**Fig. S17.** I-V curve of APTTF sample at large deformations.

Fig. S18. Resistance change to a tiny strain of 0.5% with a tensile speed of 1000 mm/min, the insets show the response and relaxation time.
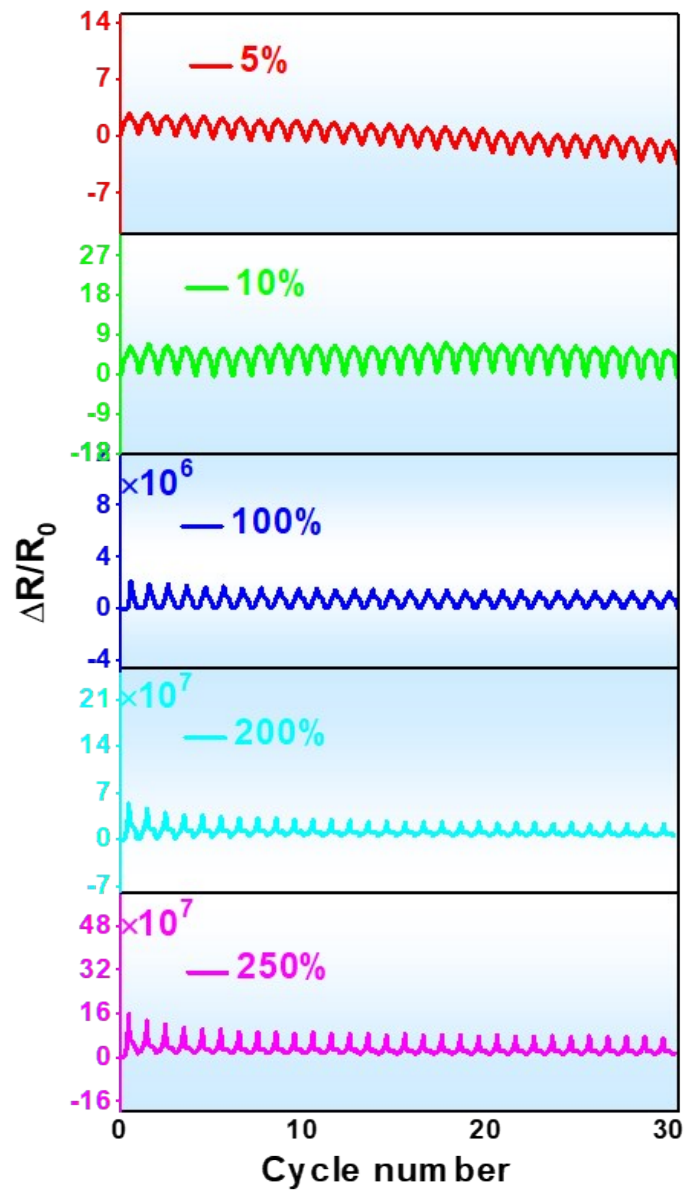
Fig. S19. $\Delta R/R_0$ change of APTTF strain sensor in 30 stretching-releasing cycles at different strains of 5%, 10%, 100%, 200%, 250%.
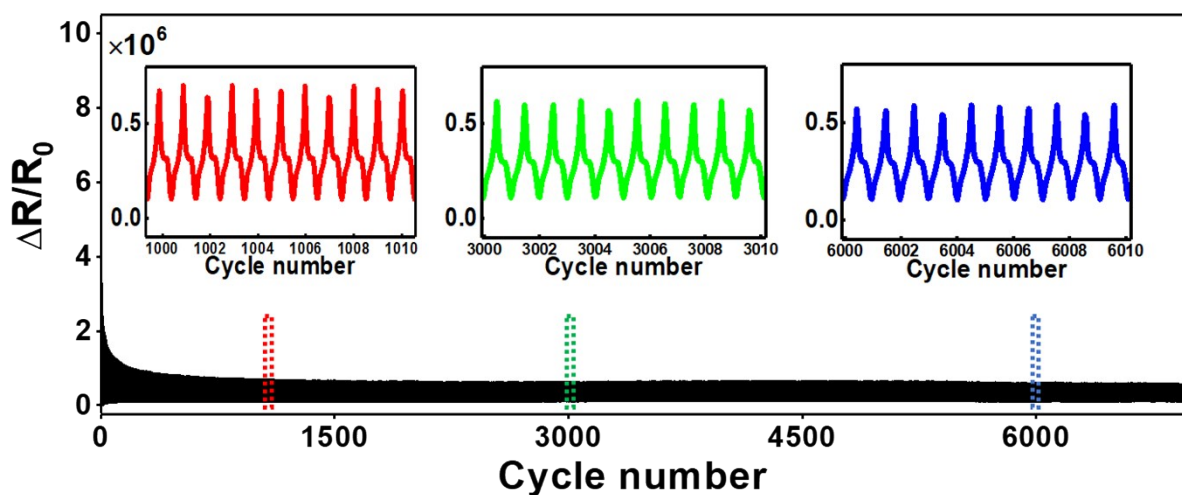
Fig. S20. Durability and stability of APTTF strain sensor in 7200 stretching-releasing cycles under 100% strain (the insets present the response signals of 1001-1010, 3001-3010, 6001-6010 cycles).

Fig. S20 illustrates the strain sensing behaviors of the fiber during 7200 cycles towards a high strain of 100% (tensile rate 100 mm/min). After undergoing reconstruction and destruction competition of the conductive network in the initial several cycles (it is primarily because of the viscoelasticity of TPU matrix), the response of APTTF turns to be stable till end of the test, showing excellent durability. The insets are magnified views of the cycles of 1001-1010, 3001-3010 and 6001-6010, respectively, from which, stable responses are also observed.
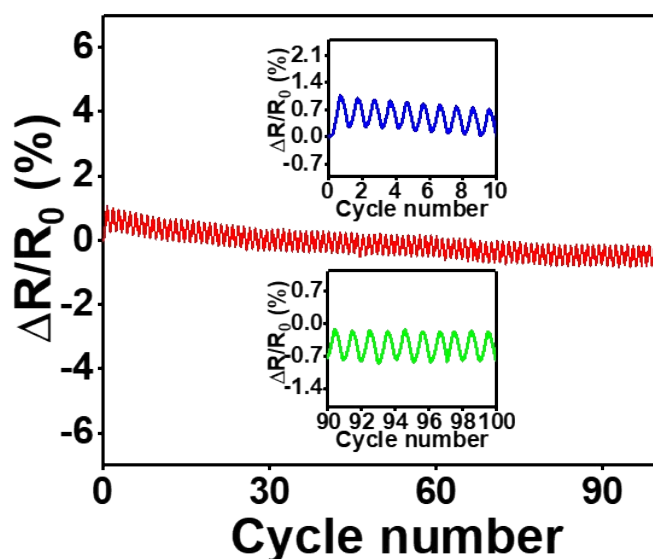
Fig. S21. Resistance change of APTTF in the temperature of 40-50 °C for 100 heating-cooling cycles (the insets display the response signals of 0-10 and 90-100 cycles).

Fig. S21 shows the temperature-resistance curve from 40 to 50 ℃ during 100 heating-cooling cycles with a rate of 10 ℃/min, excellent stability and durability are also achieved during the long-term heating-cooling test. The inserts in Fig. S21 illustrate temperature-resistance behaviors of APTTF in 0-10 and 90-100 cycles, respectively, from which well-behaved signal changes are also observed.
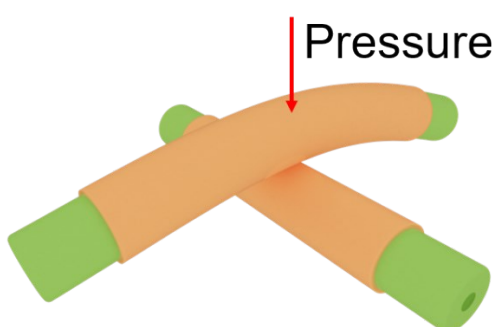
Fig. S22. The measurement setup of the single pressure sensor unit.
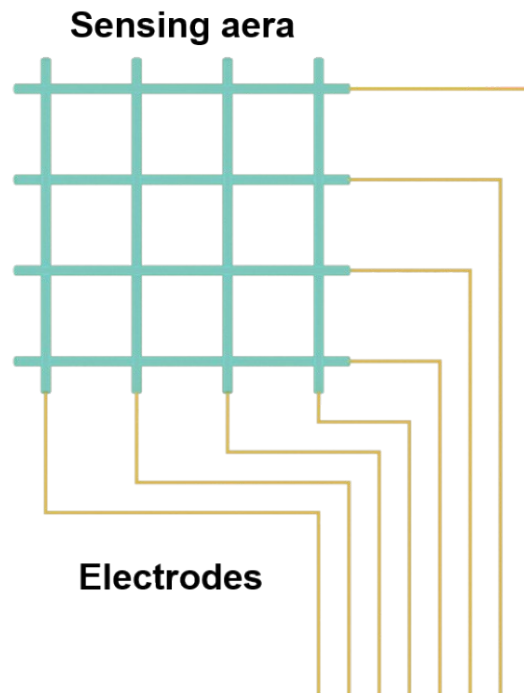
Fig. S23. Circuit diagram of the measurement of multichannel pressure sensor.
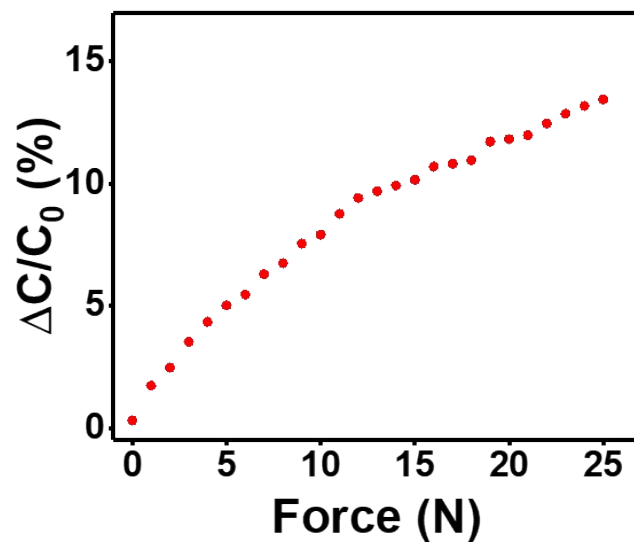
Fig. S24. The responses of capacitance at a cross point of a pressure sensing fabric.

Fig. S25. Capacitive response of the pressure sensor during compression-releasing cycles under the loadings of a) 1N; b) 2N; c) 6N; d) 10N; e) 20N; f) 25N.

Fig. S26. The reproducibility of pressure sensing to a pressure of 12N for 4000 consecutive loading-unloading cycles.

Table S1. Density and porosity of different TPU fibers.

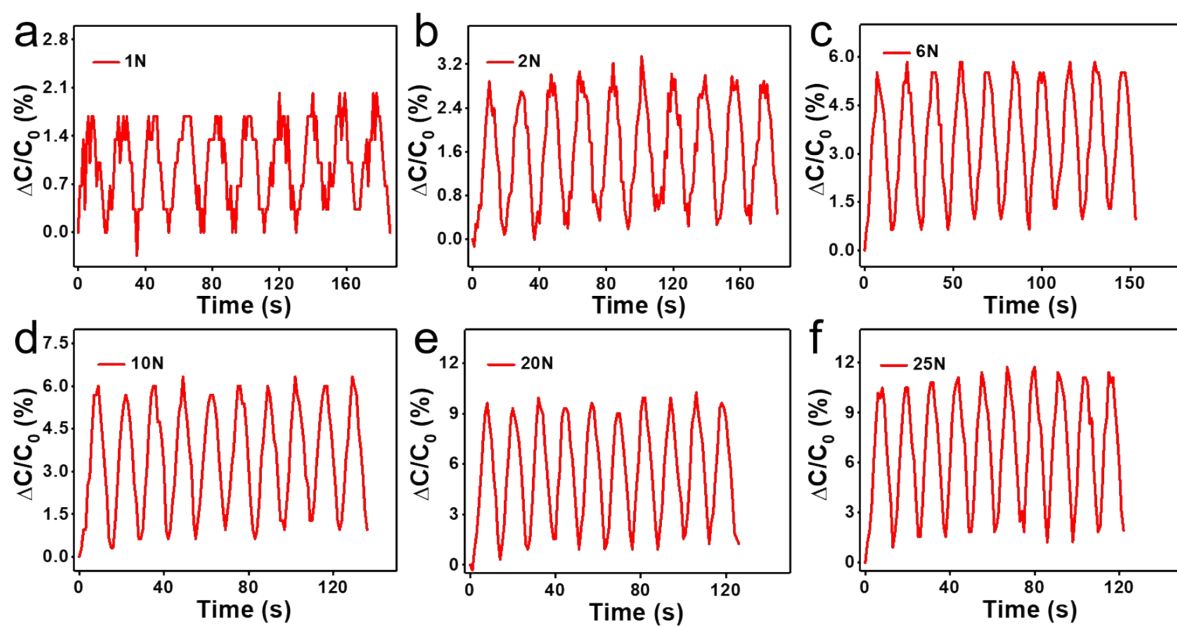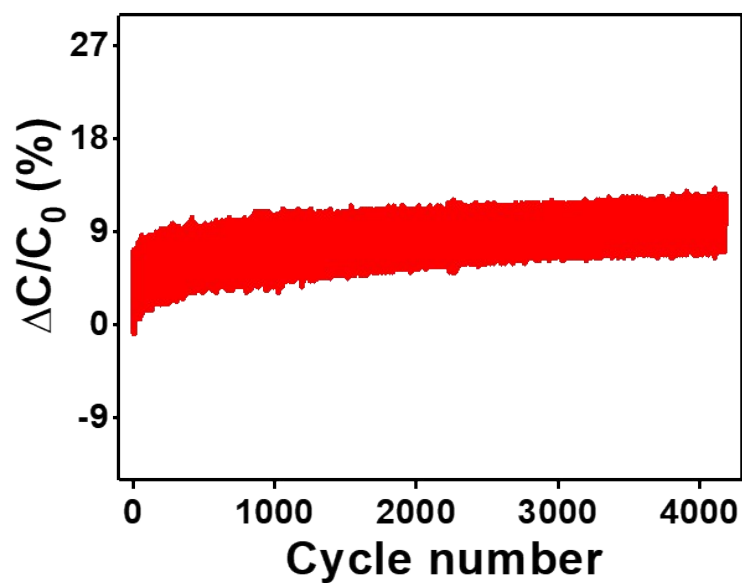| Types of TPU fiber	Density (g/cm³)	Porosity
TPU-D2.1	0.30	72.8%
TPU-D1.9	0.35	68.2%
TPU-D1.6	0.40	63.7%
TPU-D1.2	0.41	62.8%

Table S2. Thermal insulation performance comparison of our work and previous works.

Stage temperature (°C)	Type of sample	Number of Layer for textiles	Insulation performance (|ΔT|, °C)	Stretchability	Reference
-20	Silk fiber	5 layers	14		*Adv. Mater.* 2018, **30**, 1706807[1]
80	Silk fiber	5 layers	20		
-60	Kevlar fiber	1 layer	42	40%	*ACS Nano* 2019, **13**, 5703[2]
210	Kevlar fiber	1 layer	90	40%	
50	Nanocellulose fibers	5 layers	16		*Nano Energy* 2020, **68**, 104305[3]
100	Nanocellulose fibers)	5 layers	43		
150	Nanocellulose fibers	5 layers	69		
115	TPU porous fiber	1 layer	52.1	1486%	**This work**
	TPU porous fiber	2 layers	68.5		
-40	TPU porous fiber	1 layer	44		

Porosity is a parameter to defined the void spaces in a material, it is a fraction of the voids' volume, over the total volume, between 0% and 100%:

$$\Phi = \frac{\rho_0 - \rho}{\rho_0} \times 100\%$$ 　　　　　(**Equation S1**)

Where Φ is porosity, ρ_0 is the material density, and ρ is the bulk density.

Table 3. Strain sensing performance comparison of our work and previous works.

Sensitivity (GF value)	Maximum workable strain	Publication
2000	2%	*Nature.* 2014, **516**, 222[4]
1360	79%	*Adv. Mater.* 2019, **31**, 1903789[5]
7.1	100%	*Adv. Mater.* 2014, **26**, 2022[6]
75.8	50%	*Adv. Mater.* 2019, **31**, 1903130[7]
35	85%	*Adv. Mater.* 2017, **29**, 1606411[8]
37.5	500%	*Adv. Mater.* 2016, **28**, 6640[9]
5.75×10^5 (last highest record, from Prof. Zhenan Bao's group)	100%	*Sci. Adv.* 2019, **5**, eaav3097[10]
30	28%	*Sci. Robot.* 2020, **5**, eaay3604[11]
107	130%	*Nat. Commun.* 2019, **10**, 3862[12]
2.3×10^6	100%	**This work**

References

1 Y. Cui, H. Gong, Y. Wang, D. Li, H. Bai, *Adv. Mater.*, 2018, **30**, 1706807.

2 Z. Liu, J. Lyu, D. Fang, X. Zhang, *ACS Nano*, 2019, **13**, 5703.

3 J. Zhou, Y.-L. Hsieh, *Nano Energy*, 2020, **68**, 104305.

4 D. Kang, P. V. Pikhitsa, W. C. Yong, C. Lee, M. Choi, *Nature*, 2014, **516**, 222.

5 S. Gong, L. W. Yap, B. Zhu, Q. Zhai, W. Cheng, *Adv. Mater.*, 2019, **31**, 1903789.

6 C. Yan, J. Wang, We. Kang, M. Cui, Xu.Wang, *Adv. Mater.*, 2014, 26, 2022.

7 S. Pan, Z. Liu, M. Wang, Y. Jiang, Y. Luo, C. Wan, D. Qi, C. Wang, X. Ge, X. Chen, *Adv. Mater.*, 2019, **31**, 1903130.

8 Y. Cai, J. Shen, Z. Dai, X. Zang, Q. Dong, G. Guan, L. J. Li, W. Huang, X. Dong, *Adv. Mater.*, 2017, **24**, 1606411.

9 C. Wang, X. Li, E. Gao, M. Jian, K. Xia, *Adv. Mater.*, 2016, **28**, 6640.

10 J. Y. Oh, D. Son, T. Katsumata, Y. Lee, Z. Bao, *Sci. Adv.*, 2019, **5**, eaav3097.

11 S. Y. Kim, Y. Choo, R. A. Bilodeau, M. C. Yuen, G. Kaufman, D. S. Shah, C. O. Osuji, R. Kramer-Bottiglio, *Sci. Robot.*, 2020, **5**, eaay3604.

12 W. Miao, Y. Yao, Z. Zhang, C. Ma, X. Wang, *Nat. Commun.*, 2019, **10**, 3862.